Observation of disorder-driven carrier localization by Auger resonant Raman scattering in *n*-type doped ZnO

M. Sakamaki,* N. Kawai, T. Miki, T. Kaneko, T. Konishi, and T. Fujikawa
Graduate School of Advanced Integration Science, Chiba University, Chiba 263-8522, Japan

K. Amemiya and Y. Kitajima
IMSS, High Energy Accelerator Research Organization, Tsukuba, Ibaraki 305-0801, Japan

Y. Kato and T. Muro
SPring-8, JASRI, Sayo, Hyogo 679-5198, Japan

H. Yamauchi and M. Sakai
Graduate School of Engineering, Chiba University, Chiba 263-8522, Japan
(Received 22 May 2010; revised manuscript received 7 March 2011; published 26 April 2011)

We present direct evidence of carrier localization in (Zn,Al)O by using Auger resonant Raman scattering, which makes use of the competition between the core-hole decay time and the motion of the photoexcited electrons. From the branching ratio of the competing two channels, i.e., normal Auger-like and spectator Auger processes, we found that the average carrier transfer time from a donor site is in the range of 6–140 fs depending on structural disorder. The transfer time shows a rapid increase at a certain energy in the conduction band. This result suggests that the disorder-induced localization limits the electronic conductivity in the heavily *n*-doped ZnO.

DOI: 10.1103/PhysRevB.83.155210 PACS number(s): 72.80.Ng, 61.05.cj, 72.20.−i, 79.60.−i

I. INTRODUCTION

ZnO is an *n*-type semiconductor with a direct wide band gap of 3.4 eV. Here, we are interested in Al-added ZnO especially at high Al concentrations. In heavily doped semiconductors, the properties of carrier electrons are strongly affected by modification of the density of states (DOS) of the conduction band by doping, localization of the electronic states due to disorder, and electron correlations in the conduction band. The valence band of ZnO has mainly O $2p$ character. The conduction band is predominantly of Zn $4s$ character and the effective mass is comparatively small.[1] The conduction-band width of ionic semiconductors with heavy cations is mainly determined by the overlap between the outermost *s* wave functions of second-neighbor metal ions. E_F can be moved well into the conduction band by doping, and therefore the effect of disorder on the electronic conductivity is generally expected to be small.[2,3] However, the resistivity of Al-doped ZnO shows the lowest value at Al contents of ∼3–6 at.% and increases at higher Al concentrations.[4] Lu *et al*. proposed that the intragrain congregation of Al is responsible for the above behavior from the decrease of both the carrier concentration and the mobility.[5] On the other hand, as Cho *et al*. suggested from x-ray absorption and photoemission study of amorphous ZnO film, structural disorder can largely alter the electrical properties even in the absence of different phases or grain boundaries.[6] In this paper, we probe the dynamics of photoexcited electrons in the conduction band from the Zn $2p$ core level by using the Auger resonant Raman (ARR) effect. Based also on the electronic structure observed by x-ray absorption spectroscopy (XAS) and photoemission spectroscopy (PES), we discuss the interplay between electron dynamics in the conduction band and the structural disorder. The branching ratio to the ARR channel reflects the competition between the core-hole decay time and the motion of the photoexcited electrons, and has been proven to be useful in studying the electron dynamics in atoms and molecules adsorbed on surfaces.[7–9] ARR scattering is observed also in metals.[10,11] Although it can be a promising tool in studying the carrier dynamics in bulk solids, there have been only a few studies done on ARR scattering in bulk system.[12]

II. EXPERIMENTAL

Samples of (Zn,Al)O with a thickness of ∼30 nm were prepared on an indium tin oxide (ITO) film-glass substrate by rf magnetron sputtering.[13] ITO film was deposited below the sample to prevent charging in the electron yield and photoemission measurements. Samples with a thickness of ∼100 nm were also prepared directly on fused silica substrate for the fluorescence mode XAS measurements. The sputtering target was a sintered mixture of ZnO and Al_2O_3, where the content of Al changed as 0, 6, 13, 19, and 23 at.%. During the film deposition, the total working pressure was maintained at 0.4 Pa of Ar and the substrate temperature was kept at almost room temperature. Figure 1 displays the Cu $K\alpha$ x-ray-diffraction (XRD) profiles of the $Al_xZn_{1-x}O$ samples with x = 0–0.23. The (002) peak, which represents the preferential *c*-axis orientation perpendicular to the substrate,[14] was observed for the samples with 0–13 at.% Al. This peak shifts to lower angle and becomes broader with increasing Al content. The samples with 19 and 23 at.% Al were x-ray amorphous and no clear (002) peak nor peaks from other phases were observed. Figure 2 shows Al $1s$ XAS spectra at room temperature measured in the fluorescence mode. The XAS measurements were performed at beamline BL-11A, KEK-PF.[15] The XAS spectrum of α-Al_2O_3 taken from Ref. 16 is also shown for comparison. Segregation of small clusters of α-Al_2O_3 as a

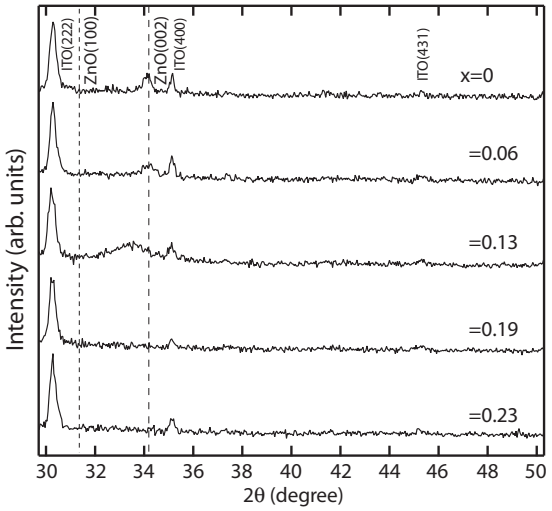

FIG. 1. XRD profiles of $Al_xZn_{1-x}O$ on an ITO film-glass substrate.

major component is excluded from this result. Recent papers point out the existence of a metastable phase of ZnO-Al_2O_3 solid solutions, which limits the electrical conductivity, at similar Al concentrations.[17–19] Although it is difficult to draw definitive conclusions concerning the existence of such phases in the present samples only from these data, correlated shifts in the valence PES and Zn $2p$, Al $1s$, and O $1s$ XAS suggest single phase rather than phase separation. Optical transmission measurements showed almost linear band-gap widening with the increase of Al concentration up to 23 at.%. This behavior is in contrast to the optical-absorption data reported by Lu *et al.* [5] At lower Al concentrations, Sernelius *et al.* [20] reported the band-gap widening in ZnO films containing up to 2 at.% Al, which can be explained by a combination of the Burstein-Moss shift and the many-body effect. The resistivity showed a minimum (∼0.5 Ω cm) at an Al concentration of 6 at.%.

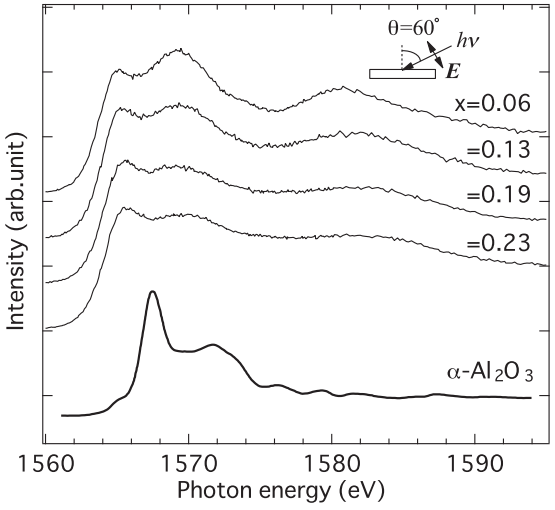

FIG. 2. Al $1s$ XAS spectra of $Al_xZn_{1-x}O$ measured in the fluorescence mode and α-Al_2O_3 taken from Ref. 16. The fluorescence measurement was performed at the grazing-incidence setup. The geometry of the measurements is shown in the panel.

The Zn $2p$ XAS measurements were performed in the total electron yield (TEY) mode at beamline BL-11A, KEK-PF. The ARR and PES experiments were performed at beamline BL27SU, SPring-8.[21] The linearly polarized light was used in all the measurements. The photon-energy resolution was set to be ∼0.2 eV, which is narrower than the core-hole lifetime width of Zn $2p_{3/2}$, which is about 0.6 eV.[22] The samples were cleaned by Ar^+ bombardment before measurement. The acceleration voltage was 0.5−4 kV at a pressure of 8×10^{-4} Pa depending on the thickness or hardness of the contaminated surface layer that is monitored by a C $1s$ PES signal. Chemical composition of ZnO is reported to be stable against Ar^+ sputtering.[23] Besides, we observed no changes in Zn $2p$ and Al $1s$ XAS spectra except for an increase of the intensity, indicating little structural damage due to the cleaning process.

III. RESULT AND DISCUSSION

Figure 3 shows valence PES and Zn $2p_{3/2}$ XAS spectra of $Al_xZn_{1-x}O$ with $x = 0$–0.23 at 100 K. PES spectra were taken at $h\nu = 1020$ eV. Calculated DOS at $x = 0$ is also shown for comparison. The calculation is based on the generalized gradient approximation (GGA) in the density-functional theory.[24] Spectral features in PES spectra are reasonably well described by calculated DOS and shift to higher binding energy with increasing Al concentration. This is consistent with the optical measurement and indicates that Al supplies electrons to the conduction band in the whole concentration range for our samples, i.e., the Fermi level E_F lies in the conduction band. However, XAS spectra show distinctly nonrigid band behavior, with the appearance of a peak around 1021–1024 eV that accompanies Al doping. In this energy region, the spectra have no angular dependence (not shown), indicating that this region contains mainly a Zn $4s$ component and corresponds to the bottom of the conduction band as in the calculated DOS. Segregated phases would not be the origin of the peak,[25] and we then interpret this change as an intrinsic property. On the other hand, the spectral features around 1024–1033 eV show a large angular dependence and can be identified as of Zn d character. These features are smeared out with increasing Al content, indicating an increase of the local structural disorder around Zn atoms. The trend in the spectral feature toward higher Al concentrations is similar to what was observed in amorphous ZnO by Cho *et al.*[6] They interpreted the peak as being caused by localized Zn $4s$ states due to weaker Zn $4s$–O $2p$ hybridization. A similar Zn $4s$ peak has also been obtained in calculated DOS of a ZnO cluster with symmetric tilt boundaries, where the localized interface-like states in the conduction band are generated, rather than deep in-gap impurity states.[26] In the following, we shall show that ARR scattering gives direct proof for the above localization hypothesis.

Figures 4(a)–4(e) shows PES spectra of $Al_xZn_{1-x}O$ around the Zn $2p_{3/2}$ threshold ($h\nu \sim 1021$ eV). The Zn $3d^8$ final-state features lie between a binding energy of 27 and 50 eV. A normal Auger-like component, whose kinetic energy is constant, was seen above the threshold. This decay process is expressed as $2p^53d^{10} \rightarrow 2p^63d^8 + e^-$, as shown in Fig. 5(a). On the other hand, a resonant Auger component, whose binding energy is constant, was seen between $h\nu = 1020$ and 1026 eV.

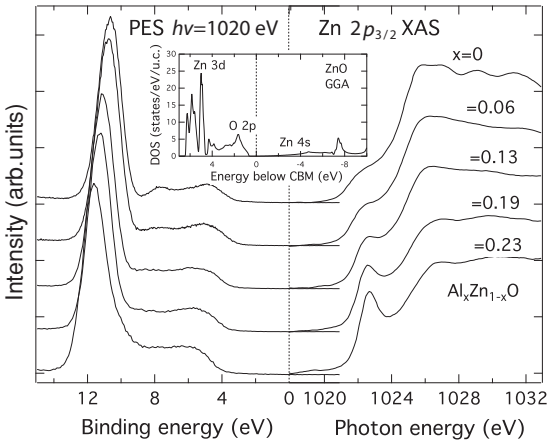

FIG. 3. Zn $2p_{3/2}$ XAS and valence PES spectra of $Al_xZn_{1-x}O$ at 100 K. Inset: GGA DOS of ZnO.

The resonant excitation and subsequent decay take place as a one-step process in the resonant Auger process. There are two possible resonant processes, which are called spectator Auger and participator Auger processes. In the former process, the excited electron remains in unoccupied states, while in the latter process, it recombines with the core hole. The spectator process gives ARR scattering, and its final state is Zn $3d^84s^1$. If the electron stays in localized states in a narrow energy range in the conduction band [shaded region in Fig. 5(b)(i)] after the initial excitation, the kinetic energy of the electron shows almost linear dispersion with the incident photon energy. This results in constant binding energy for the spectator Auger process. Direct photoemission from a mixed d^{10} and d^9 ground state by configuration interaction (CI) can also give a $3d^84s^1$ final state. The d^9 final state lies at a binding energy of ~11 eV in Fig. 4, and can be reached by a participator Auger and direct photoemission channel from the Zn $3d$ band. Therefore,

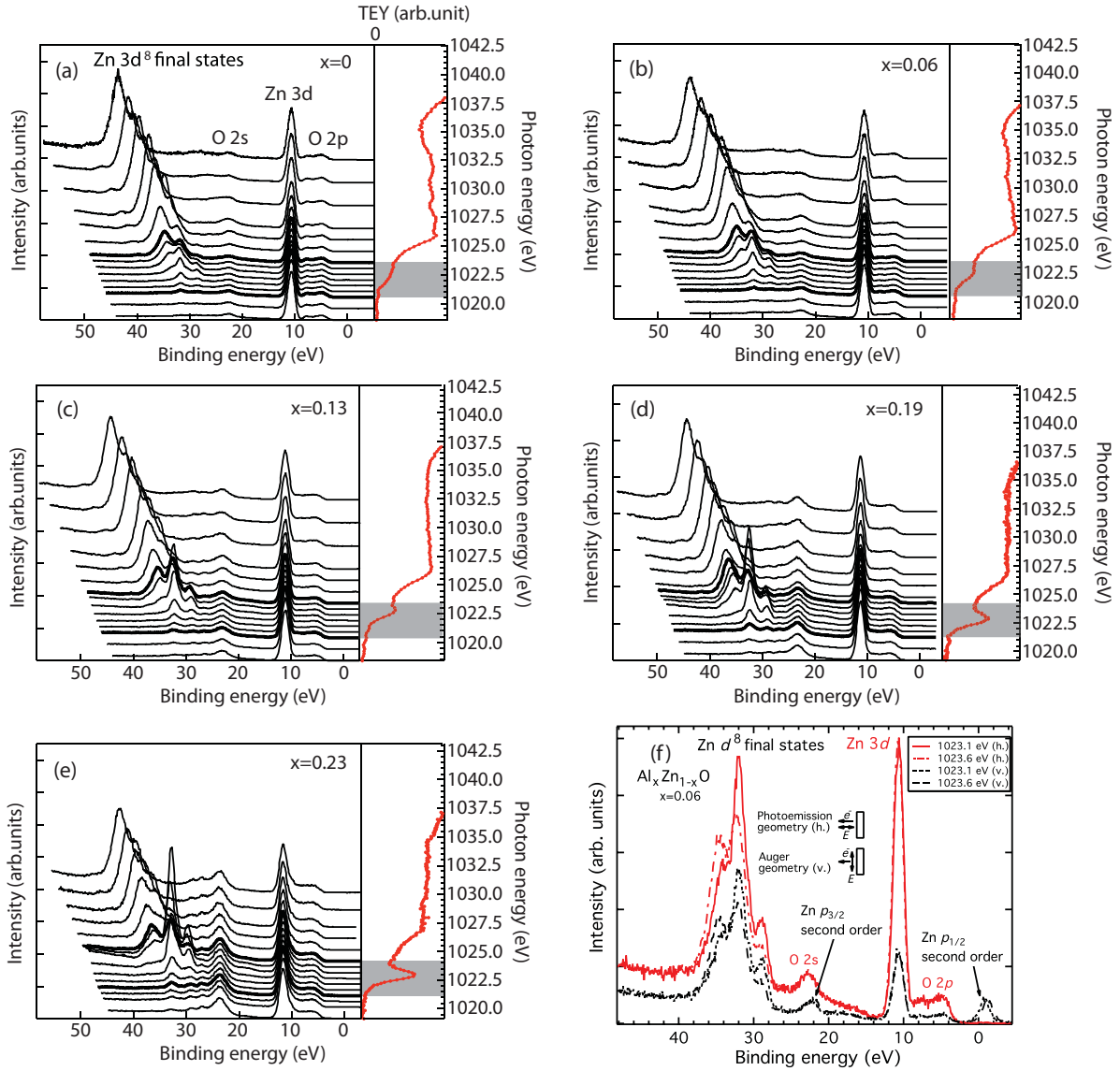

FIG. 4. (Color online) (a)–(e) Resonant PES spectra of $Al_xZn_{1-x}O$. Photon energy was varied through Zn $2p_{3/2}$ threshold. Thicker lines indicate the shaded energy region in XAS spectra. (f) Polarization dependence of PES spectra of the sample with $x = 0.06$ at $h\nu = 1023.1$ and 1023.6 eV.

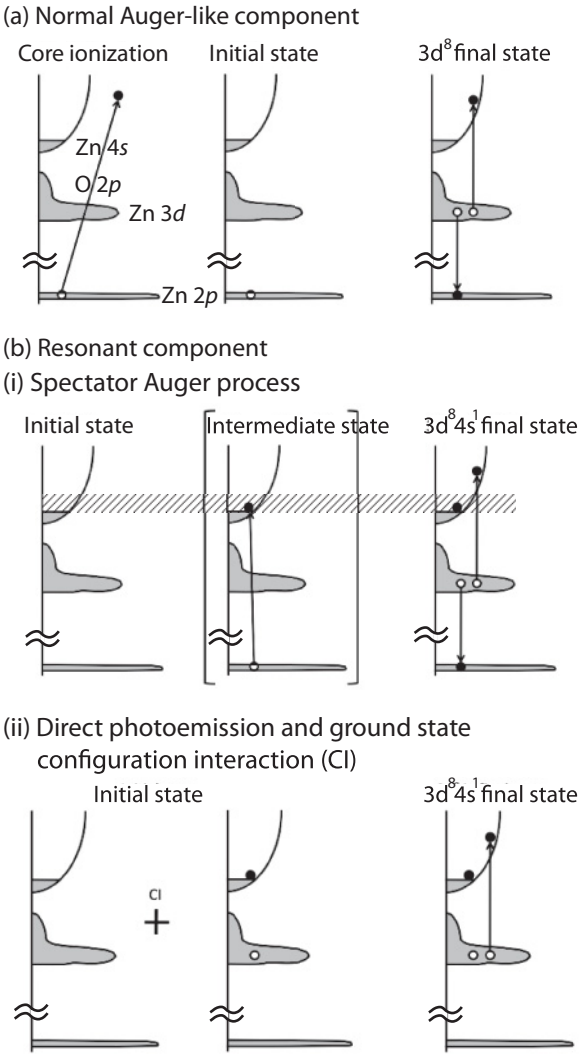

FIG. 5. Schematic description of normal Auger decay, resonant Auger, and direct photoemission processes. (a) Core-hole decay gives Zn $3d^8$ final state with a total charge of +2 in the case of normal Auger process. (b) The Zn $3d^8$ final states with total charge +1 can be reached by two channels: (i) spectator Auger process, via intermediate state with a core hole, and (ii) direct photoemission from mixed d^{10} and d^9 ground states by configuration interaction.

the following two possible processes can contribute to the resonant component in Fig. 4: (i) ARR scattering, i.e., spectator Auger process, $2p^6 3d^{10} \rightarrow 2p^5 3d^{10} 4s^1 \rightarrow 2p^6 3d^8 4s^1 + e^-$, and/or (ii) direct photoemission and ground state CI[10], $2p^6 3d^{10} \xrightarrow{\text{CI}} 2p^6 3d^9 4s^1 \rightarrow 2p^6 3d^8 4s^1 + e^-$, as shown in Fig. 5(b). The intensity of the resonant component increases with increasing Al concentration. For samples with higher Al concentrations, the intensity of the resonant component was much larger than the normal component near the threshold and showed a maximum near the peak energy in XAS. This is direct evidence that the photoexcited electrons in the intermediate state become localized if the direct photoemission channel (ii) can be neglected.

To estimate how much the direct photoemission channel (ii) contributes to the constant binding-energy part of the d^8 final-state spectra, we measured the incident x-ray polarization dependence. Figure 4(f) shows a polarization dependence of PES spectra for $Al_xZn_{1-x}O$ with $x = 0.06$ at $h\nu = 1023.1$ and 1023.6 eV. These photon energies are in the shaded region of the XAS spectrum in Fig. 4(b), where the intensity and the line shape of the d^8 component in the PES spectra are sensitive to a small change of the photon energy. The photoelectrons were collected in the horizontal plane using horizontally polarized x rays (h., photoemission geometry) or vertically polarized x rays (v., Auger geometry) where the direct photoemission should be suppressed. There are no significant differences in the photon-energy dependence of the line shape and the intensity between the two geometries. This indicates that the contribution of the direct photoemission to the d^8 final state is negligible and the spectator contribution (i) is dominant. Similar behavior has been observed in Cu metal.[10]

Peak-area analysis of the PES spectra provides the branching ratio in the decay channel of the Zn $2p_{3/2}$ core-hole states. This can be translated into the carrier transfer time τ_{ct} of electron hopping to the neighboring sites if we adopt a simple two-step picture for the spectator Auger process. In the case of Zn $2p$ excitation, the intermediate state is $[2p^5\, 3d^{10} +$ (excited electron)], i.e., Zn^{2+} with a core hole and an extra electron in the conduction band. From the viewpoint of the $(Z + 1)$ approximation, this is equivalent to *a 3+ ion of group III impurity plus a donor electron*, i.e., Ga^{3+} and an electron at the donor site. Thus, we observe the equivalent of the dynamics of a donor electron from a group III donor.

To decompose the overlapping d^8 final state into two components, we performed a fitting procedure as follows. Figure 6(a) shows the fit of the d^8 final-state spectra of undoped ZnO at $h\nu = 1032.6$ eV, where only the normal Auger component was seen. The line shape can be fitted

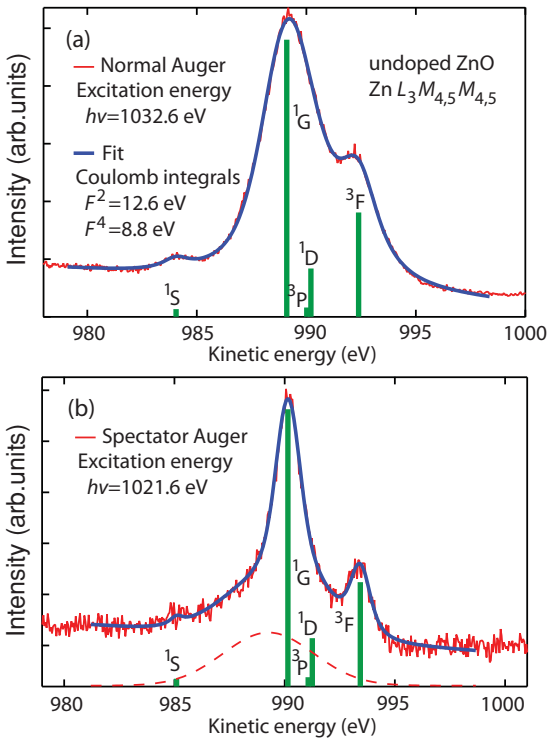

FIG. 6. (Color online) Fit of the d^8 final-state spectra of undoped ZnO at (a) $h\nu = 1032.6$ eV and (b) 1021.6 eV.

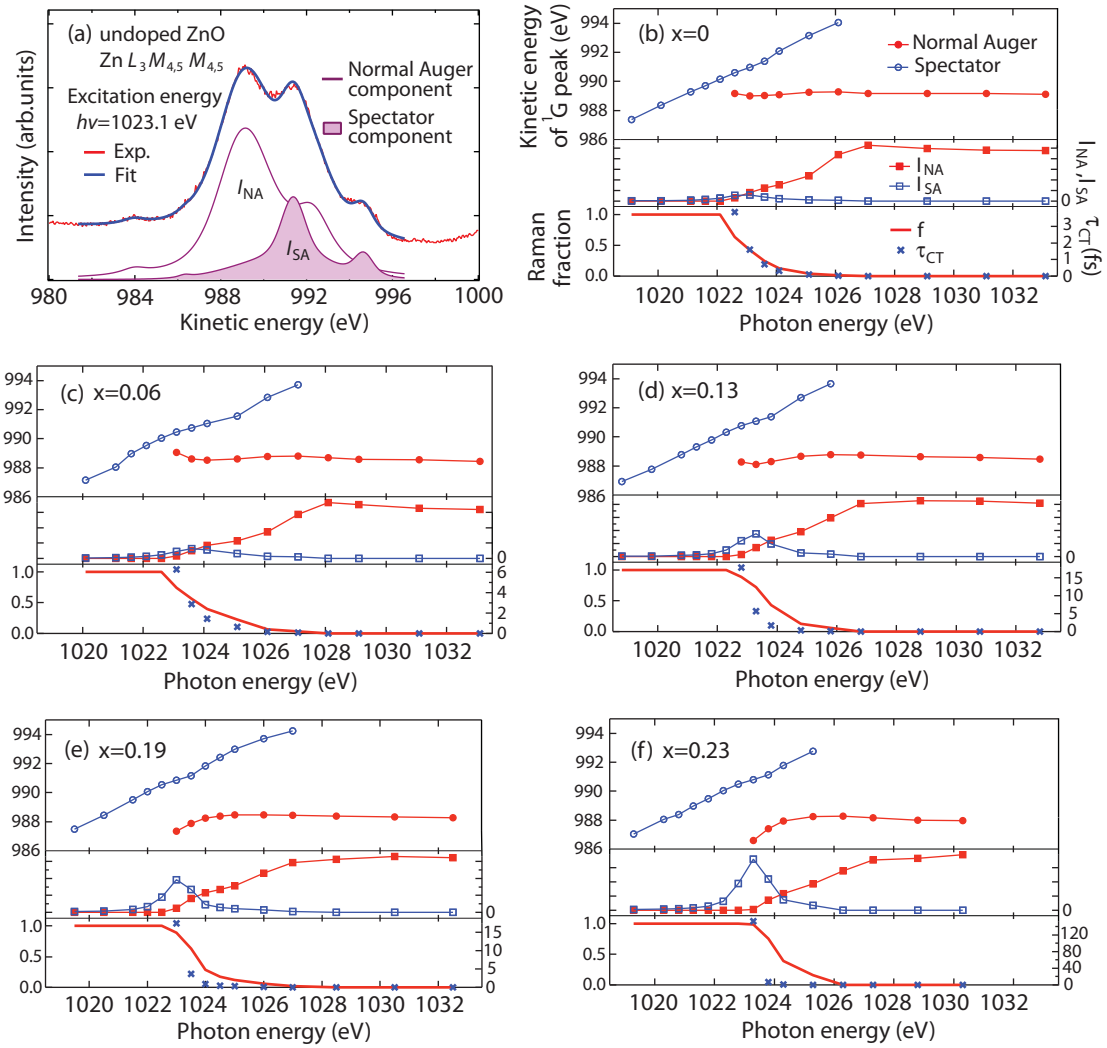

FIG. 7. (Color online) (a) Decomposition of the d^8 final-state spectrum of undoped ZnO at $h\nu = 1023.1$ eV into normal Auger-like and spectator components. (b)–(f) Quantitative carrier transfer time analysis of $Al_xZn_{1-x}O$. In each panel, top: Kinetic energy of the ^1G peak as a function of incoming photon energy, middle: intensities (I_{NA} and I_{SA}), bottom: Raman fraction f and carrier transfer time τ_{ct}.

by the d^8 multiplet with theoretical transition probability.[27] The theoretical spectra consist of ^1S, ^1G, ^3P, ^1D, and ^3F Zn $3d^8$ final-state atomic multiplet terms. The Coulomb integrals F^2 and F^4 are used as parameters in the fit. Regarding the spectator component, a similar fit was performed using the spectrum at 1021.6 eV, where only the resonant component was observed [Fig. 6(b)]. There are differences from theoretical values in the intensity distribution of the multiplet terms, and it is necessary to add a broad contribution in the case of a spectator component. Using these Coulomb integrals and the widths of the multiplet lines, the series of the d^8 final-state spectra are decomposed into normal Auger-like and spectator components. As an example, the decomposition of the d^8 final-state spectrum of undoped ZnO at $h\nu = 1023.1$ eV is shown in Fig. 7(a).

Figures 7(b)–7(f) show the result of the decomposition. In the upper part of each panel, the kinetic energy of the ^1G peak is plotted. The component that appears above $h\nu = 1022$ eV and shows nearly constant kinetic energy corresponds to the normal Auger-like component. The other component, whose kinetic energy approximately follows the incoming photon energy, corresponds to the spectator component. The integrated intensities of normal Auger-like and spectator components, I_{NA} and I_{SA}, are plotted in the middle part of each panel. I_{NA} increases from the threshold and follows the XAS line shape (see Fig. 3). I_{SA} has appreciable values only in the region of 1021–1025 eV. From these results, XAS spectra can be decomposed into two components. One of them, which has a smooth edge shape, corresponds to the transition to the spatially extended states in the conduction band before the core-hole decay. In this case, the photoelectron does not feel the strong core-hole potential and the line shape of this component represents the relatively unperturbed DOS of the conduction band. The onset of this component corresponds to the Fermi level in the case of high Al concentration and degenerate samples. Another component comes from the spectator process, where the photoelectron stays near the x-ray absorbing atom.

The intensity ratio $f = I_{SA}/(I_{SA} + I_{NA})$ can be translated to the Zn site-averaged carrier transfer time as $\tau_{ct} = \tau\, f/(1 - f)$ using the core-hole lifetime τ [2.2 fs in the case of Zn

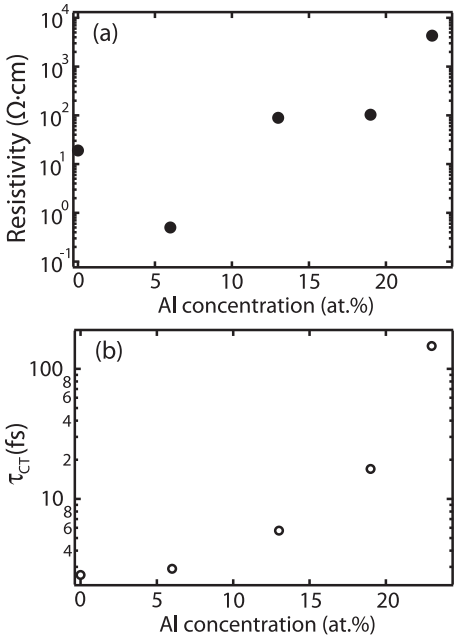

FIG. 8. (a) Electrical resistivity as a function of Al content. (b) τ_{ct} at the energy where I_{SA} shows maximum.

$2p_{3/2}$ (Ref. 22)] as an internal clock.[7] In the bottom part of Figs. 7(b)–7(f), the intensity ratio or Raman fraction f and τ_{ct} are plotted. For undoped ZnO, τ_{ct} is ∼4 fs at the threshold and has smaller values at higher energies in the conduction band. The carrier transfer time τ_{ct} near E_F becomes longer by increasing Al content. The obtained τ_{ct} is in the range of 6–140 fs. This increase can be interpreted as localization of electronic states in the conduction band. As a function of energy, τ_{ct} shows a rapid increase near E_F. The energy positions of this rapid increase in the samples with high Al concentration indicate that in those samples, states near E_F are localized and the conduction is through hopping rather than metallic. The Al concentration dependence of τ_{ct} indicates that the increase of the disorder by increasing the amount of Al leads to localization of the electronic states in the conduction band.

Figure 8 shows the electrical resistivity and τ_{ct} as functions of Al content. τ_{ct} values at the energy where the intensity of the spectator component I_{SA} shows a maximum are plotted here. τ_{ct} is related to the dynamics of an electron at a donor impurity site as mentioned above, and τ_{ct} does not necessarily correlate directly with the dynamics of the electrons at the Fermi level, which determines macroscopic electrical conductivity. Nevertheless, it is still interesting to inspect the correlation between them. Going from 0 to 6 at.%, the resistivity decreases and τ_{ct} does not show a large change. In this region, the conductivity is dominated by the increase of the number of the carriers, and is not affected much by disorder-induced localization. At Al concentration above 6 at.%, both τ_{ct} and the resistivity increase. In particular at higher Al concentrations, both τ_{ct} and the resistivity increase by one order of magnitude between the samples with an Al content of 13 and 23 at.%. In general, the conductivity depends on the carrier concentration and the mobility. Lu *et al.* reported a similar conductivity decrease at Al contents >4 at.% together with a decrease of both the carrier concentration and the mobility.[5] In contrast to the result by Lu *et al.*, optical, PES, and XAS measurements on the samples in the present study showed band-gap widening, which can be interpreted as filling of the conduction band to the highest Al concentrations. If that is the case, the decrease of the mobility, not the decrease of the carrier density, must account for the resistivity increase at Al contents >6 at.%. The present result suggests that the localization of carrier electrons due to structural disorder explains the decrease of the mobility. Although the relationship between τ_{ct} and the mobility is still not established at present, being a local and microscopic quantity, τ_{ct} should be useful in the understanding of physical processes that determine the electrical conductivity.

It is interesting to note that the energy positions of the normal Auger-like component in $x = 0.19$ and 0.23 show different behavior near the threshold. They deviate from the constant kinetic energy and show the Raman-like constant binding energy. This indicates that the two-step description for the normal Auger-like components is no longer valid for these cases.

IV. CONCLUSION

We probed the dynamics of excited electrons in the conduction band by using the branching ratio to the ARR scattering channel, and we found that the carrier transfer time near E_F in the conduction band is in the range of 6–140 fs depending on the amount of Al. This is direct evidence of the disorder-induced localization of the electronic states in the conduction band. This localization determines the carrier mobility in the case of ZnO with structural disorder, in contrast to ionic semiconductors with heavier metal ions. This also highlights the core-hole clock technique as a useful tool in elucidating the carrier dynamics in semiconductors in the time scale of a femtosecond or less.

ACKNOWLEDGMENTS

We thank T. Kinoshita for discussion and technical support at SPring-8. This work was financially supported by the Global COE program (Advanced School for Organic Electronics, Chiba University), and performed under the approval of the Photon Factory Program Advisory Committee (2007G214) and the SPring-8 budding researchers support program (2008A1718).

*Present address: IMSS, High Energy Accelerator Research Organization, Tsukuba, Ibaraki 305-0801, Japan; masako.sakamaki@kek.jp

[1] Y. N. Xu and W. Y. Ching, Phys. Rev. B **48**, 4335 (1993).
[2] R. Martins, P. Barquinha, L. Pereira, I. Ferreira, and E. Fortunato, Appl. Phys. A **89**, 37 (2007).

[3]H. Hosono, J. Non-Cryst. Solids **352**, 851 (2006).
[4]T. Minami, H. Nanto, and S. Takata, J. Appl. Phys. **23**, L280 (1984).
[5]J. G. Lu, Z. Z. Ye, Y. J. Zeng, L. P. Zhu, L. Wang, J. Yuan, B. H. Zhao, and Q. L. Liang, J. Appl. Phys. **100**, 073714 (2006).
[6]D.-Y. Cho, J. H. Kim, K. D. Na, J. Song, C. S. Hwang, B.-H. Park, J.-Y. Kim, C.-H. Min, and S.-J. Oh, Appl. Phys. Lett. **95**, 261903 (2009).
[7]P. A. Brühwiler, O. Karis, and N. Mårtensson, Rev. Mod. Phys. **74**, 703 (2002).
[8]A. Föhlisch, P. Feulner, F. Hennies, A. Fink, D. Menzel, D. Sanchez-Portal, P. M. Echenique, and W. Wurth, Nature (London) **436**, 373 (2005).
[9]D. Menzel, Chem. Soc. Rev. **37**, 2212 (2008).
[10]A. Föhlisch, O. Karis, M. Weinelt, J. Hasselström, A. Nilsson, and N. Mårtensson, Phys. Rev. Lett. **88**, 027601 (2001).
[11]M. Weinelt, A. Nilsson, M. Magnuson, T. Wiell, N. Wassdahl, O. Karis, A. Föhlisch, N. Mårtensson, J. Stöhr, and M. Samant, Phys. Rev. Lett. **78**, 967 (1997).
[12]E. Carleschi, M. Malvestuto, M. Zacchigna, A. Nicolaou, V. Brouet, S. Hébert, H. Muguerra, D. Grebille, and F. Parmigiani, Phys. Rev. B **80**, 035114 (2009).
[13]H. Iechi, T. Okawara, M. Sakai, M. Nakamura, and K. Kudo, Electr. Eng. Jpn. **158**, 49 (2007).
[14]JCPDS, International Centre for Diffraction Data, No. 36-1451.
[15]Y. Kitajima, Y. Yonamoto, K. Amemiya, H. Tsukabayashi, T. Ohta, and K. Ito, J. Electron Spectrosc. Relat. Phenom. **101-103**, 927 (1999).
[16]D. Cabaret, P. Sainctavit, P. Ildefonse, and A.-M. Flank, J. Phys. Condens. Matter **8**, 3691 (1996).
[17]S. Yoshioka, F. Oba, R. Huang, I. Tanaka, T. Mizoguchi, and T. Yamamoto, J. Appl. Phys. **103**, 014309 (2008).
[18]M. Vinnichenko, R. Gago, S. Cornelius, N. Shevchenko, A. Rogozin, A. Kolitsch, F. Munnik, and W. Moller, Appl. Phys. Lett. **96**, 141907 (2010).
[19]D. Horwat, M. Jullien, F. Capon, J.-F. Pierson, J. Andersson, and J. L. Endrino, J. Phys. D **43**, 132003 (2010).
[20]B. E. Sernelius, K.-F. Berggren, Z.-C. Jin, I. Hamberg, and C. G. Granqvist, Phys. Rev. B **37**, 10244 (1988).
[21]H. Ohashi, E. Ishiguro, Y. Tamenori, H. Kishimoto, M. Tanaka, M. Irie, T. Tanaka, and T. Ishikawa, Nucl. Instrum. Methods Phys. Res., Sect. A **467-468**, 529 (2001).
[22]J. C. Fuggle and S. F. Alvarado, Phys. Rev. A **22**, 1615 (1980).
[23]R. Kelly, Nucl. Instrum. Methods **149**, 553 (1978).
[24]P. Blaha, K. Schwarz, G. K. H. Madsen, D. Kvasnicka, and J. Luiz, *WIEN2k* (Karlheinz Schwarz, Tchn. Universität Wien, Austria, 2001).
[25]The whole spectra including the appeared peak showed an upward shift that was larger in the heavily doped samples when the temperature was raised (not shown).
[26]F. Oba, I. Tanaka, S. R. Nishitani, H. Adachi, B. Slater, and D. H. Gay, Philos. Mag. A **80**, 1567 (2000).
[27]E. Antonides, E. C. Janse, and G. A. Sawatzky, Phys. Rev. B **15**, 1669 (1977).